Archives of Biochemistry and Biophysics 475 (2008) 25–35

Contents lists available at ScienceDirect

Archives of Biochemistry and Biophysics

journal homepage: www.elsevier.com/locate/yabbi

Grb2 adaptor undergoes conformational change upon dimerization

Caleb B. McDonald [a], Kenneth L. Seldeen [a], Brian J. Deegan [a], Marc S. Lewis [b], Amjad Farooq [a,*]

[a] Department of Biochemistry and Molecular Biology and the UM/Sylvester Braman Family Breast Cancer Institute, Leonard Miller School of Medicine, University of Miami, Gautier Building, Room 214, 1011 NW 15th Street, Miami, FL 33136, USA

[b] Molecular Interactions Resource, Laboratory of Bioengineering and Physical Science, National Institute of Biomedical Imaging and Bioengineering, National Institutes of Health, Bethesda, MD 20892, USA

ARTICLE INFO

Article history:
Received 5 March 2008
and in revised form 7 April 2008
Available online 14 April 2008

Keywords:
Grb2 dimerization
Isothermal titration calorimetry
Analytical ultra-centrifugation
Size-exclusion chromatography
Mass spectrometry

ABSTRACT

Grb2 is an adaptor protein that couples activated receptor tyrosine kinases to downstream effector molecules such as Ras and Akt. Despite being a central player in mitogenic signaling and a target for therapeutic intervention, the role of Grb2 oligomerization in cellular signaling is not well understood. Here, using the techniques of size-exclusion chromatography, mass spectrometry, analytical ultra-centrifugation and isothermal titration calorimetry, we demonstrate that Grb2 exists in monomer–dimer equilibrium in solution and that the dissociation of dimer into monomers is entropically-driven without an unfavorable enthalpic change at physiological temperatures. Our data indicate that enthalpy and entropy of dimer dissociation are highly temperature-dependent and largely compensate each other resulting in negligible effect of temperature on the overall free energy. From the plot of enthalpy change versus temperature, the magnitude of heat capacity change derived is much smaller than that expected from the rather large molecular surfaces becoming solvent-occluded upon Grb2 dimerization, implying that Grb2 monomers undergo conformational rearrangement upon dimerization. 3D structural models of Grb2 dimer and monomers suggest strongly that such conformational rearrangement upon dimerization may arise from domain swapping. Taken together, our study provides novel insights into the role of Grb2 as an adaptor in cellular signaling circuitry and how Grb2 dimerization may impart high fidelity in signal transduction as well as lead to rapid signal amplification upon receptor stimulation.

Grb2[1] is a ubiquitous component of cell signaling networks that couples activated receptor tyrosine kinases (RTKs) to downstream effectors and regulators. The critical role of Grb2 in cellular signaling is exquisitely demonstrated through defects in mice embryos upon the disruption of *grb2* gene [1]. Grb2 is a modular protein comprised of a central SH2 domain flanked between an N-terminal SH3 (nSH3) domain and a C-terminal SH3 (cSH3) domain, giving it an overall modular architecture of nSH3–SH2–cSH3 [2]. Grb2 recognizes activated RTKs by virtue of its SH2 domain to bind to tyrosine-phopshorylated (pY) sequences in the context of the consensus motif pYXN located within the cytoplasmic tails of a diverse array of receptors, including EGF and PDGF receptors [3,4]. Alternatively, Grb2 can also indirectly dock onto activated RTKs through the binding of its SH2 domain to pY sequences within the adaptor protein p52Shc [5,6]. Given a much broader spectrum of RTKs recognized by p52Shc, Grb2 is more often seen to fulfill this latter role instead of directly binding to RTKs upon receptor stimulation. For its part, p52Shc contains at least two well-conserved YXN motifs at positions Y239 and Y317 that are subject to phosphorylation by a diverse array of protein tyrosine kinases, including the Src kinase family, upon its recruitment to receptor tails in response to extracellular mitogenic stimuli [7–9]. It has been shown that phosphorylation of both Y239 and Y317 in p52Shc is required for efficient recruitment of Grb2 to the inner membrane surface [10]. Could this necessity be explained by the ability of Grb2 to participate in cellular signaling as a dimer?

Upon the interaction of Grb2 to RTKs directly or indirectly, the SH3 domains of Grb2 present a placid opportunity for a wide variety of proteins, containing proline-rich sequences, to be recruited to the inner membrane surface and thus engage in downstream cellular signaling cascades. Some of the best characterized downstream partners of Grb2 SH3 domains are the guanine nucleotide exchange factor Sos1 [11,12], the adaptor protein Gab1 [13,14], the endocytic GTPase dynamin1 [15,16], the ubiqui-

* Corresponding author. Fax: +1 305 243 3955.
E-mail address: amjad@farooqlab.net (A. Farooq).

[1] *Abbreviations used:* AUC, analytical ultra-centrifugation; EGF, epidermal growth factor; Grb2, growth factor receptor binder 2; ITC, isothermal titration calorimetry; MALDI-TOF, matrix-assisted LASER desorpton/ionization-time of flight; MAPK, mitogen-activated protein kinase; MMCO, molecular mass cut-off; PDGF, platelet-derived growth factor; RTK, receptor tyrosine kinase; SASA, solvent-accessible surface area; SEC, size-exclusion chromatography; SH2, Src homology 2; SH3, Src homology 3; Shc, Src homology containing.

0003-9861/$ - see front matter © 2008 Elsevier Inc. All rights reserved.
doi:10.1016/j.abb.2008.04.008

tin ligase Cbl [14,17,18] and the cell cycle inhibitor p27kip1 [19]. Upon recruitment to the inner membrane surface, these downstream effectors of Grb2 exert a wide multitude of biological responses. For example, Sos1 catalyzes the GDP-GTP exchange within the small membrane-bound GTPase Ras and thereby switches on a key signaling circuit that involves the activation of MAPK cascade central to cellular proliferation, survival and differentiation [20,21]. Likewise, the recruitment of Gab1 provides docking platforms for the protein tyrosine phosphatase Shp2 and the lipid kinase PI3K, which respectively account for further amplification of Ras activity, as sustained activation of Ras requires both the Sos1-dependent and Gab1-dependent pathways [22–24], and the activation of serine-threonine kinase Akt/PKB, which plays a pivotal role in cell growth and survival [25]. The recruitment of dynamin1 to the inner membrane surface is believed to trigger clathrin-mediated receptor endocytosis of EGFR—a key mechanism for initiating intracellular signaling [26,27]. In contrast, the recruitment of Cbl to the p52Shc–Grb2 signaling complex at the inner membrane surface results in ubiquitination of EGFR and its subsequent degradation, a step that is critical for negating the oncogenic potential of EGFR [28]. Finally, the recruitment of p27kip1 to the Shc–Grb2 signaling complex appears to negatively regulate the activity of Ras by virtue of its ability to compete with Sos1 for binding to Grb2 [19].

Grb2 is architecturally one of the simplest and smallest adaptor proteins with an overall modular architecture of nSH3–SH2–cSH3 [2]. The availability of its complete 3D structure has rendered Grb2 a prototype for understanding the function of other adaptor proteins in cellular signaling [29]. In the 3D crystal structure of Grb2, the protein crystallized as a dimer with twofold axis of symmetry such that the SH2 domain of one monomer docks against the cSH3 domain of the other and vice versa in a head-to-tail fashion [29]. In this manner, the ligand-binding sites in the SH2 and the SH3 domains remain fully exposed to solution and thereby rendering Grb2 in an active state and fully primed to participate in cellular signaling within the dimeric assembly. To paraphrase this slightly, the role of Grb2 dimerization appears to stabilize the protein further rather than providing a negative regulatory switch that may need to be invoked upon receptor stimulation. Such a dimeric assembly of Grb2 is also expected to eliminate the need for any conformational change prior to interaction with upstream RTKs or downstream effector molecules. The extent to which Grb2 dimerization prevails in solution and the extent to which the monomers may have to undergo conformational change upon dimerization is however not clear. Does Grb2 dimerize in solution? Do the monomers come together as rigid bodies to generate the Grb2 dimer or do they have to undergo some sort of conformational change upon dimerization?

To address these key issues, we undertook the present study. Here, using the techniques of size-exclusion chromatography, mass spectrometry, analytical ultra-centrifugation and isothermal titration calorimetry, we demonstrate that Grb2 exists in monomer–dimer equilibrium in solution and that the dissociation of dimer into monomers is entropically-driven without an unfavorable enthalpic change at physiological temperatures. Our data further indicate that the heat capacity change is much smaller than that expected from the rather large molecular surfaces becoming solvent-occluded upon Grb2 dimerization, implying that Grb2 monomers undergo conformational rearrangement upon dimerization. 3D structural models of Grb2 dimer and monomers suggest strongly that such conformational rearrangement upon dimerization may arise from domain swapping. Taken together, our study provides novel insights into the role of Grb2 as an adaptor in cellular signaling circuitry and how Grb2 dimerization may impart high fidelity in signal transduction as well as lead to rapid signal amplification upon receptor stimulation.

Materials and methods

Protein preparation

Full-length human Grb2 (residues 1–217; Expasy# P62993) was cloned into pET102 bacterial expression vector with an N-terminal thioredoxin (Trx)-tag followed by a thrombin site (a total of 133 additional residues at the N-terminus) and a C-terminal polyhistidine (His)-tag preceded by a thrombin site (a total of 36 additional residues at the C-terminus) using Invitrogen TOPO technology. Trx-tag was included to maximize protein expression in soluble fraction, while the His-tag was added to aid in protein purification by Ni–NTA affinity chromatography. Additionally, thrombin protease sites were introduced at both the N- and C-termini of the protein to aid in the removal of tags after protein purification. Proteins were subsequently expressed in *Escherichia coli* Rosetta2 (DE3) bacterial strain (Novagen) cultured in LB media and purified on Ni–NTA affinity column using standard procedures. Further treatment of the protein on a MonoQ ion-exchange column and a Hiload Superdex200 size-exclusion column coupled to GE Akta FPLC system led to purification of recombinant Grb2 to apparent homogeneity as judged by SDS–PAGE analysis. The identity of recombinant Grb2 was further confirmed by MALDI-TOF mass spectrometry analysis. Protein yield was typically between 20 and 30 mg of recombinant Grb2 of apparent homogeneity per liter of bacterial culture. The treatment of recombinant protein with thrombin protease significantly destabilized Grb2 and rendered it proteolytically unstable. For this reason, all experiments reported herein were carried out on a 43-kDa recombinant fusion Grb2 (386 residues) containing a Trx-tag at the N-terminus and a His-tag at the C-terminus. The tags were found to have no effect on the functional properties of Grb2. Protein concentrations were determined by both fluorescence using Invitrogen Quant-It assay and absorbance at 280 nm using an extinction co-efficient of 52,160 $M^{-1}cm^{-1}$ for the recombinant Grb2. The extinction co-efficient was calculated from amino acid sequence alone using the online software ProtParam at ExPasy Server [30]. Results from both methods were in an excellent agreement.

SEC analysis

Size-exclusion chromatography (SEC) on recombinant Grb2 was performed using a Hiload Superdex200 column coupled to a GE Akta FPLC system equipped with the UNICORN software for automatic operation. After purification to apparent homogeneity using Ni–NTA affinity chromatography and ion-exchange chromatography, recombinant Grb2 was extensively dialyzed in 50 mM Tris, 200 mM NaCl, 1 mM EDTA and 5 mM β-mercaptoethanol at pH 8.0. The recombinant protein was concentrated to 100–300 μM using Amicon Ultra-15 centrifugal filter units (MMCO 30 kDa) prior to application on Superdex200 column pre-equilibrated in the same buffer at 4 °C. The elution of protein was recorded using UV monitor at 280 nm and automatically plotted as a function of elution volume in the UNICORN software. The identity of Grb2 in elution fractions was further confirmed by SDS–PAGE, Western blotting and MALDI-TOF mass spectrometry analysis. The apparent molecular mass of recombinant Grb2 was obtained by extrapolation of its recorded elution volume on a straight line graph generated by plotting the logarithm of the molecular mass of known protein markers versus their elution volumes on the Superdex200 column pre-equilibrated in the same buffer at 4 °C. Control experiments involving the analysis of thioredoxin containing a C-terminal His-tag on the Superdex200 column confirmed that the tags possessed no oligomeric potential.

MALDI-TOF mass spectrometry

Matrix-assisted LASER desorption/ionization-time of flight (MALDI-TOF) mass spectrometry analysis of recombinant Grb2 was performed on a Voyager-DE spectrometer with a linear detector coupled to v.5.0 software from Applied Biosystems. Recombinant Grb2 was extensively dialyzed in 10 mM Tris and 5 mM β-mercaptoethanol at pH 8.0. The dialyzed protein solution was mixed with an equal volume of matrix solution and the resulting mixture was air-dried on the sample plate prior to MALDI-TOF analysis. The matrix solution comprised of a saturated solution of 3,5-dimethoxy-4-hydroxycinnamic acid in acetonitrile/water (1:1). Molecular masses were calibrated externally with bovine serum albumin. Molecular mass accuracy was within ±0.25%. All MALDI-TOF experiments were carried out at the Global Peptide Services, Fort Collins, CO.

AUC experiments

Analytical ultra-centrifugation (AUC) sedimentation equilibrium experiments were carried out in a Beckman–Coulter XL-A analytical ultracentrifuge at rotor speeds of 17,000 rpm at 4 °C. After purification to apparent homogeneity using Ni–NTA affinity chromatography and ion-exchange chromatography, recombinant Grb2 was extensively dialyzed in 50 mM Tris and 200 mM NaCl at pH 8.0 prior to transfer to an ultracentrifuge cell at various initial concentrations in the range 0.1–10 μM. The distribution of Grb2 concentration, expressed as absorbance at 280 nm (A_r), as a function of radius (r) at centrifugal equilibrium was analyzed

using $L-1$ (robust) regression with the mathematical modeling system MLAB (Civilized Software, Silver Spring, MD) and was best fit to the following equation based on a reversible monomer–dimer equilibrium model:

$$A_r = A_b \exp\left[M\omega^2(1-\bar{\nu}\rho)(r^2-r_b^2)/2RT\right] + A_b^2 \times \exp\left[\ln K_a - \ln(\varepsilon/2) + 2M\omega^2(1-\bar{\nu}\rho)(r^2-r_b^2)/2RT\right] + \delta \quad (1)$$

where A_b is the absorbance at 280 nm at the radial position r_b (at the cell bottom), ϵ the molar extinction co-efficient of the monomer at 280 nm, M is the molecular mass of the monomer, ω is the angular velocity of the rotor, $\bar{\nu}$ is the partial specific volume of the monomer, ρ is the buffer density, R is the universal molar gas constant, T is the absolute temperature, K_a is the equilibrium association constant for dimer formation and δ is the baseline offset. The above analysis was carried out globally for various monomer-equivalent concentrations of Grb2 in the range 0.1–10 μM.

ITC measurements

Isothermal titration calorimetry (ITC) experiments were performed on Microcal VP-ITC instrument and data were acquired and processed using fully automized features in Microcal ORIGIN software. All measurements were repeated 3–4 times. Briefly, after purification to apparent homogeneity using a combination of Ni–NTA affinity chromatography, ion-exchange chromatography and size-exclusion chromatography, recombinant Grb2 was extensively dialyzed in either Tris buffer (50 mM Tris, 200 mM NaCl, 1 mM EDTA and 5 mM β-mercaptoethanol at pH 8.0), or alternatively, in Phosphate buffer (50 mM sodium phosphate, 200 mM NaCl, 1 mM EDTA and 5 mM β-mercaptoethanol at pH 8.0). The protein samples were subsequently concentrated to 100–300 μM using the Amicon Ultra-15 centrifugal filter units (MMCO 30 kDa) and de-gassed using the ThermoVac accessory for 10 min. The experiments were initiated by injecting 25×10 μl injections of 100–300 μM of recombinant Grb2 from the syringe into the calorimetric cell containing 1.8 ml of the same buffer, used for protein dialysis, at a fixed temperature in the narrow range 10–30 °C. The change in thermal power as a function of each injection was automatically recorded using Microcal ORIGIN software and the raw data were further processed to yield binding isotherms of heat uptake per injection as a function of monomer concentration. The heats of mixing and dilution were subtracted from the heat of dimer dissociation per injection by carrying out a control experiment in which the appropriate buffer in the calorimetric cell was titrated against concentrated thioredoxin containing a C-terminal His-tag (Trx-His) from the syringe in an identical manner. Control experiments involving the injection of concentrated Trx-His into the appropriate buffer alone or containing Grb2 in the calorimetric cell produced similar heats to those observed for the injection of buffer into buffer, implying that neither Trx-tag nor His-tag interacts with Grb2. To extract various thermodynamic parameters, the binding isotherms were iteratively fit in Microcal Origin using non-linear least squares-regression analysis to the following sigmoidal function:

$$q(i) = \Delta H/\{1+\exp[(C-K_d)/f]\} \quad (2)$$

where $q(i)$ is the heat uptake (kcal/mol) for the ith injection (the Y-axis variable), C is the total monomer-equivalent concentration of the dimer (μM) injected into the calorimetric cell after ith injection (the X-axis variable), ΔH is the total enthalpy of dimer dissociation (kcal/mol), K_d is the apparent equilibrium dissociation constant of the dimer (μM) and f is the steepness factor (μM), related to the number of moles of dimer injected per unit volume of the calorimetric cell for the ith injection, of the sigmoidal curve for the dissociation of Grb2 dimer into monomers. The above model is the simplest mathematical function that best describes our data and the resulting fit directly generated the thermodynamic parameters K_d and ΔH for the dissociation of Grb2 dimer into monomers. The free energy change (ΔG) upon dimer dissociation was calculated from the relationship:

$$\Delta G = RTlnK_d \quad (3)$$

where R is the universal molar gas constant (1.99 cal/K/mol), T is the absolute temperature in Kelvins and K_d is in the units of mol/L. The entropic contribution ($T\Delta S$) to the free energy of binding was calculated from the relationship:

$$T\Delta S = \Delta H - \Delta G \quad (4)$$

where ΔH and ΔG are as defined above. Heat capacity change (ΔC_p) upon dimer dissociation was calculated by measuring ΔH as a function of temperature (T) in the narrow range 10–30 °C with the slope of the ΔH versus T plot yielding the value of ΔC_p.

SASA calculations

The magnitude of polar and apolar solvent-accessible surface area (SASA) becoming occluded upon the formation of Grb2 dimer from monomers was calculated from thermodynamic data and compared to that determined from the 3D structures of Grb2 dimer and monomers [29].

For calculation of change in polar SASA ($\Delta SASA_{polar}$) and apolar SASA ($\Delta SASA_{apolar}$) upon Grb2 dimerization from thermodynamic data, it was assumed that ΔC_p and ΔH at 60 °C (ΔH_{60}) are additive and linearly depend on the change in $\Delta SASA_{polar}$ and $\Delta SASA_{apolar}$ as embodied in the following empirically-derived expressions [31–34]:

$$\Delta C_p = a[\Delta SASA_{polar}] + b[\Delta SASA_{apolar}] \quad (5)$$

$$\Delta H_{60} = c[\Delta SASA_{polar}] + d[\Delta SASA_{apolar}] \quad (6)$$

where a, b, c and d are empirically-determined co-efficients with values of −0.14 cal/mol/K/Å^2, +0.32 cal/mol/K/Å^2, +31.34 cal/mol/Å^2 and −8.44 cal/mol/Å^2, respectively. The co-efficients, a and b are independent of temperature, while c and d refer to a temperature of 60 °C, which equates to the median melting temperature of the proteins from which these constants are derived [31–33]. ΔC_p for the dissociation of Grb2 dimer was calculated from the slope of a plot of ΔH versus T in the narrow temperature range 10–30 °C using ITC instrument. ΔH_{60} for the dissociation of Grb2 dimer was calculated by extrapolation of a plot of ΔH versus T in the narrow temperature range 10–30 °C, using ITC instrument, to 60 °C. With ΔC_p and ΔH_{60} experimentally determined using ITC and the knowledge of co-efficients a–d from empirical models [31–34], Eqs. (5) and (6) were simultaneously solved to obtain the magnitudes of $\Delta SASA_{polar}$ and $\Delta SASA_{apolar}$ independent of structural information upon the dissociation of Grb2 dimer into monomers.

Changes in $\Delta SASA_{polar}$ and $\Delta SASA_{apolar}$ upon Grb2 dimerization from 3D structural data were calculated using the following relationships:

$$\Delta SASA_{polar} = [SASA_{dp}] - 2[SASA_{mp}] \quad (7)$$

$$\Delta SASA_{apolar} = [SASA_{da}] - 2[SASA_{ma}] \quad (8)$$

where $SASA_{dp}$ and $SASA_{da}$ are the polar and apolar SASA of Grb2 dimer, and $SASA_{mp}$ and $SASA_{ma}$ are the polar and apolar SASA of Grb2 monomer. $SASA_{dp}$ and $SASA_{da}$ were calculated from the 3D structural model of Grb2 dimer (see below), $SASA_{mp}$ and $SASA_{ma}$ were calculated from the 3D structural model of Grb2 monomer assuming it retained the same conformation as that observed in the dimer for the Rigid Body model (see below), while $SASA_{mp}$ and $SASA_{ma}$ were calculated from the 3D structural model of Grb2 monomer assuming it adopted a different conformational when in isolation for the Flexible Body model (see below). All SASA calculations were performed using the online software GETAREA with a probe radius of 1.4 Å [35].

Structural modeling

3D structures of Grb2 monomers alone and as a dimer were modeled using the MODELLER software based on homology modeling [36]. The model of Grb2 dimer was obtained using the crystal structure of Grb2, but lacking residues 28–33 in a loop in the nSH3 domain as a result of lack of electron density, as a template (with a PDB code of 1GRI). The Rigid Body model of Grb2 monomer, assuming it retained the same conformation as that observed in the dimer, was obtained using atomic coordinates of only one monomer in the crystal structure of Grb2 (with a PDB code of 1GRI). The Flexible Body model of Grb2 monomer, assuming it adopted a different conformation when in isolation, was obtained using atomic coordinates of nSH2 and cSH3 domains of one monomer and the atomic coordinates of SH2 domain from the other monomer in the crystal structure of Grb2 (with a PDB code of 1GRI). In the Flexible Body model of Grb2 monomer, the residues in the inter-domain loops were allowed to float freely without a template so as to enable them to adopt the energy-minimized conformations consistent with the re-arrangement of the SH2 domain relative to nSH3 and cSH3 domains. In each case, a total of 100 structural models were calculated and the structure with the lowest energy, as judged by the MODELLER Objective Function, was selected for further energy minimization in MODELLER prior to analysis. The structures were rendered using the RIBBONS software [37]. All calculations were performed on the lowest energy structural model.

Results and discussion

Grb2 exists in monomer–dimer equilibrium

In an attempt to determine the extent to which Grb2 may dimerize in solution, we analyzed the oligomeric state of full-length recombinant Grb2 on Superdex200 column using size-exclusion chromatography (SEC). Our SEC analysis reveals that Grb2 exists in two distinct species with apparent molecular masses of 43 and 90 kDa (Fig. 1a). The molecular mass of recombinant Grb2 obtained from its amino acid sequence analysis is 43.3 kDa. Thus, the most straightforward interpretation of our data is that the two species of Grb2, as observed in our SEC analysis, most likely represent the monomeric and dimeric states of the protein in agreement with the crystal structure of Grb2 [29]. To shed further light on the dimerization of Grb2, we analyzed the potential of monomeric and dimeric species to exchange with each other.

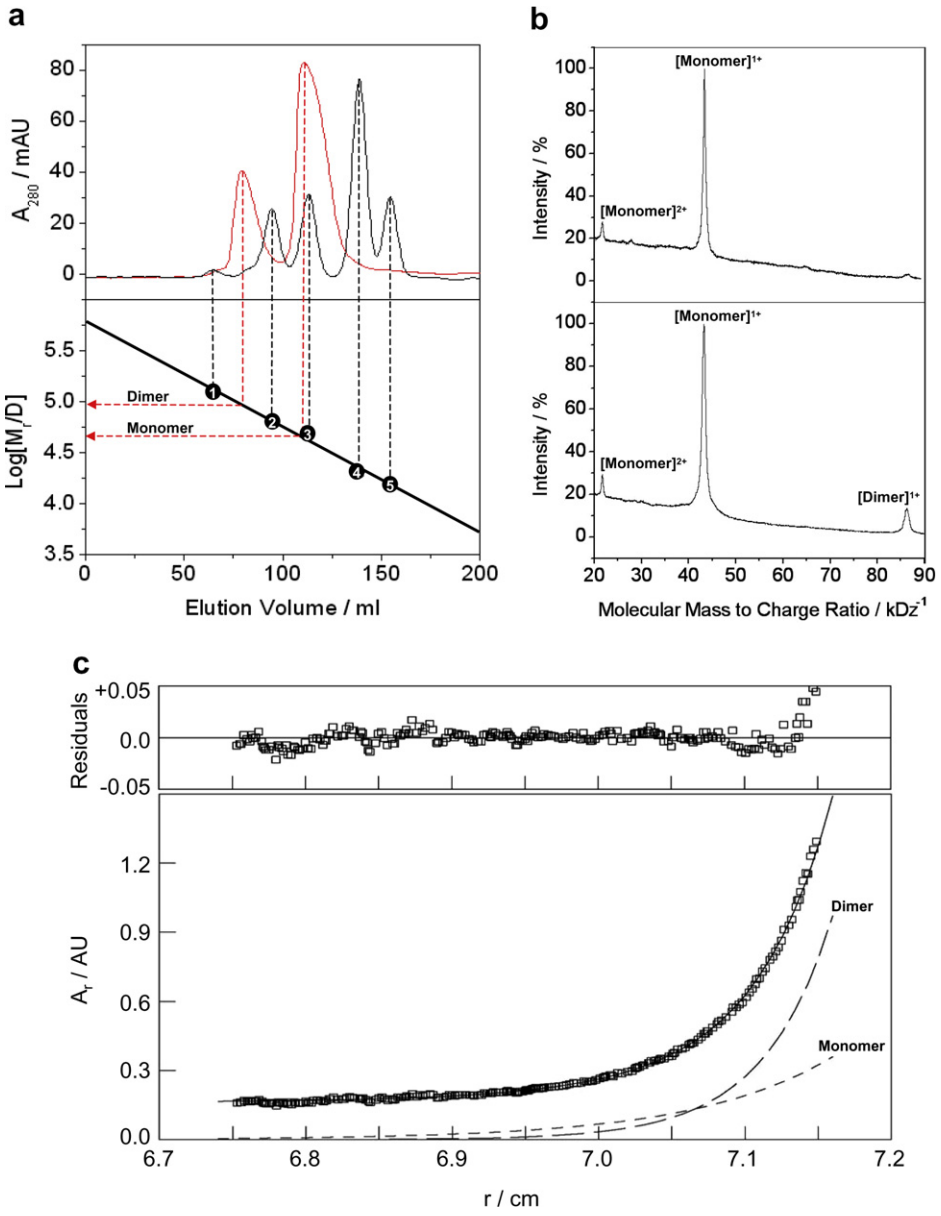

Fig. 1. Biophysical analysis of monomer–dimer equilibrium in Grb2. (a) SEC analysis of Grb2 oligomerization. Protein markers of known molecular masses or recombinant Grb2 were applied onto a Hiload Superdex200 column coupled to a GE AKTA FPLC system. The proteins were eluted with the same buffer and the elution profiles for protein markers (black) and Grb2 (red) were recorded with a UV monitor at 280 nm (top). A plot of the logarithm of the molecular mass of known protein markers versus their elution volume was fit to a straight line using linear regression analysis (bottom). The numerals indicate the elution volumes of protein markers of known molecular masses as follows: (1) 128-kDa dimeric albumin; (2) 64-kDa monomeric albumin; (3) 48-kDa ovalbumin; (4) 20-kDa chymotrypsinogen; and (5) 16-kDa ribonuclease. Extrapolation of the elutions volumes of Grb2 peaks (red) observed in the elution profile (top) on the logarithmic plot (bottom) yielded apparent molecular masses of 90 and 43 kDa—which are in remarkable agreement with the calculated molecular masses of dimeric (86.6 kDa) and monomeric (43.3 kDa) recombinant Grb2. (b) MALDI-TOF analysis of Grb2 oligomerization. SEC fractions eluting as an apparent monomer (top) and as an apparent dimer (bottom) were further subjected to MALDI-TOF mass spectrometry. The multiply charged ions of Grb2 monomer and dimer observed in the MALDI-TOF analysis are indicated. (c) AUC analysis of Grb2 oligomerization. Distribution of Grb2 concentration, expressed as absorbance at 280 nm (A_r) as a function of radius (r) at centrifugal equilibrium in the cell at a rotor speed of 17,000 rpm at 4 °C (open squares) is shown in the lower panel. The data shown are for the initial concentration of 10 μM of Grb2 loaded into the centrifugal cell. The solid line in the lower panel shows the fit of the data to a reversible monomer–dimer model using Eq. (1). The quality of the fit is indicated by the residuals shown in the upper panel. The net distribution of Grb2 observed experimentally was decomposed into the distribution of individual monomer (short dash) and dimer (long dash) as shown in the lower panel. The monomer and dimer distributions shown are not corrected for baseline offset The baseline correction was found to be approximately proportional to the initial loadings for all cells and thus appears to primarily represent non-sedimentable absorbance, although some may be artifactual. The contribution of non-sedimentable absorbance is apparent from its value at the initial point of the total gradient. (For interpretation of the references to color in this figure legend, the reader is referred to the web version of this paper.)

The species eluting as an apparent dimer and as an apparent monomer were recovered and concentrated separately and then re-injected onto Superdex200 column. Both species generated elution profiles containing a mixture of monomeric and dimeric species, implying that Grb2 exists in reversible monomer–dimer equilibrium. Although SEC analysis is highly dependent upon molecular shape, the knowledge that Grb2 is a compact globular protein with a tightly packed 3D structure speaks volumes in support of our conclusion that the two species with apparent molecular masses of 43 and 90 kDa observed here most likely represent Grb2 in its monomeric and dimeric conformation.

In support of the observation that Grb2 may exist in monomer–dimer equilibrium, we also performed MALDI-TOF analysis on the two species of Grb2 observed in SEC analysis (Fig. 1b). MALDI-TOF

analysis of the species eluting as an apparent monomer led to observation of a dominant ion of 43.3 kDa and a less dominant ion of 21.7 kDa, implying that these ions correspond to singly-charged Grb2 monomer and doubly-charged Grb2 monomer, respectively. In contrast, MALDI-TOF analysis of the species eluting as an apparent dimer led to observation of a dominant ion of 43.3 kDa and less dominant ions with molecular masses of 21.7 kDa and 86.5 kDa, implying that the dominant ion corresponds to singly-charged Grb2 monomer, while the less dominant ions correspond to doubly-charged Grb2 monomer and singly-charged Grb2 dimer, respectively. Non-covalent protein dimers do not usually survive the MALDI-TOF process but the fact that we have been able to observe Grb2 dimer in such an analysis suggests that Grb2 dimer must be a highly stable species despite its rapid exchange with its monomeric counterpart.

To further analyze the ability of Grb2 to dimerize, we carried out sedimentation equilibrium experiments using analytical ultracentrifugation (AUC) at various concentrations of Grb2 in the range 0.1–10 μM (Fig. 1c). The distribution of Grb2 concentration as a function of centrifugal radius in these experiments could not be described by either a homogeneous monomer or dimer but gave excellent fits to a reversible monomer–dimer equilibrium model. Our results thus demonstrate unequivocally that Grb2 exists in monomer–dimer equilibrium at all concentrations analyzed and that there is no evidence of the presence of any higher-order protein aggregate. The global analysis of the distribution of Grb2 at various protein concentrations in the ultracentrifuge cell at equilibrium using the monomer–dimer model, as described by Eq. (1), yielded a value of 5 μM for the apparent dimer dissociation constant (K_d) at 4 °C.

Entropy drives the dissociation of Grb2 dimer into monomers

To characterize the Grb2 monomer–dimer equilibrium in thermodynamic terms, we employed the powerful technique of isothermal titration calorimetry (ITC). Because thermodynamic parameters can be dependent upon the varying ionization of particular buffers, we performed our ITC measurements in both Tris and Phosphate buffers.

Our ITC data indicate that the dissociation of Grb2 dimer into monomers is under entropic control and accompanied by an unfavorable gain of enthalpy (Fig. 2). It has been suggested that the sigmoidal nature of ITC isotherms may result from the dissociation of higher-order multimers into dimers and monomers [38]. In light of the fact that Grb2 only exists in monomer–dimer equilibrium as evidenced by our SEC, MALDI-TOF and AUC analysis (Fig. 1), we attribute this sigmoidal behavior to the rather weak nature of Grb2 dimers. For such weak dimers, the first few injections in an ITC experiment will be expected to result in similar heat uptake due to the fact that every dimer injected into the calorimetric cell will completely dissociate. However, as the concentration of the monomers in the calorimetric cell rises after the first few injections, the additional injections will progressively result in the lowering of heat uptake due to the decreased tendency of dimers to dissociate into monomers. The heat uptake will eventually level out as the concentration of monomers reaches in excess of the dimer dissociation constant toward the final few injections. Such dissociation of weak dimers will be expected to generate a sigmoidal response curve. In contrast, the ITC isotherms will be expected to obey hyperbolic behavior for the dissociation of strong dimers—each successive injection at the start of an ITC experiment will be expected to result in a slightly lower heat uptake due to the tendency of dimers not to fully dissociate even at lower monomer concentrations in the calorimetric cell. The heat uptake will continue to decrease slowly with further injections and eventually level out as the concentration of monomers in the calorimetric cell reaches beyond the dimer dissociation constant.

To extract various thermodynamic parameters, the ITC isotherms were best fit to a sigmoidal function given in Eq. (2), assuming a model-independent approach to the analysis of dissociation of Grb2 dimer into monomers. Table 1 presents the results of such an analysis. As shown in Table 1, the dissociation of Grb2 dimer into monomers exhibits thermodynamic signatures in both Tris and Phosphate buffers that are virtually indistinguishable. Although the possibility that enthalpy change could also be a driv-

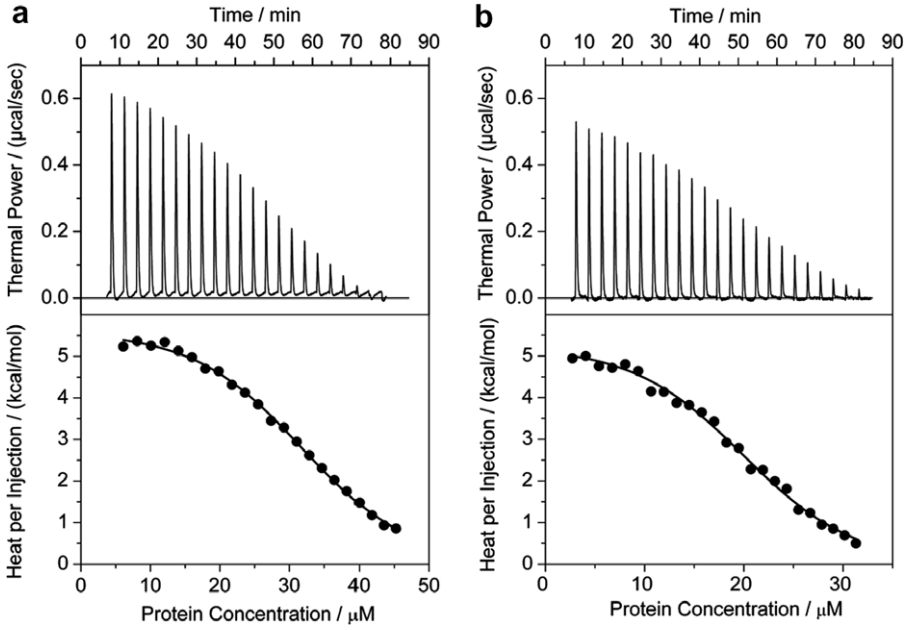

Fig. 2. ITC analysis of the dissociation of Grb2 dimer into monomers. (a) Three hundred micromolar monomer-equivalent Grb2 in Tris buffer in the injection syringe were diluted by making 25× 10 μl injections into the calorimetric cell containing the same buffer at 25 °C. (b) Two hundred micromolar monomer-equivalent Grb2 in Phosphate buffer in the injection syringe were diluted by making 25× 10 μl injections into the calorimetric cell containing the same buffer at 25 °C. In each case, protein concentration on the *x*-axis is the monomer-equivalent of Grb2 monomers formed upon Grb2 dissociation. The first injection and the corresponding heat uptake are not shown due to systematic uncertainties in the measurement. The solid lines represent the fit of the data to the sigmoidal function given in expression (2).

Table 1
Experimentally determined thermodynamic parameters for the dissociation of Grb2 dimer obtained from ITC measurements at 25 °C in Tris and Phosphate buffers

	K_d (μM)	ΔH (kcal mol^{-1})	$T\Delta S$ (kcal mol^{-1})	ΔG (kcal mol^{-1})
Tris	31.0 ± 0.9	+5.57 ± 0.35	+11.73 ± 0.35	−6.16 ± 0.02
Phosphate	19.6 ± 0.4	+5.40 ± 0.17	+11.80 ± 0.17	−6.43 ± 0.01

The values for the various parameters were obtained from the fit of the sigmoidal function given in Eq. (2) to the binding isotherms shown in Fig. 2. Errors were calculated from three to four independent measurements. All errors are given to one standard deviation. Tris buffer was 50 mM Tris, 200 mM NaCl, 1 mM EDTA and 5 mM β-mercaptoethanol at pH 8.0. Phosphate buffer was 50 mM Sodium phosphate, 200 mM NaCl, 1 mM EDTA and 5 mM β-mercaptoethanol at pH 8.0.

ing force cannot be ruled out, the dissociation of protein dimers into monomers has been hitherto observed to be an exclusively entropy-driven affair accompanied by unfavorable enthalpic changes [38–40]. Such unfavorable enthalpic changes are believed to result from the disruption of an extensive network of electrostatic interactions, hydrogen bonding and hydrophobic forces at the monomer–monomer interface upon dimer dissociation. The crystal structure of Grb2 dimer indeed shows the burial of large hydrophobic surface area upon dimerization and it is thus likely that the unfavorable gain in enthalpy observed here is due to the disruption of intermolecular interactions at the monomer–monomer interface [29].

What might be the molecular basis of favorable entropic contributions to the free energy upon the dissociation of Grb2 dimer into monomers? Net entropic changes upon the dissociation of protein dimer into monomers are likely to result from interplay between the following three major entropic forces ΔS_{solv}, ΔS_{conf} and ΔS_{mix}. ΔS_{solv} is the unfavorable entropy change due to reduction in the degrees of freedom of solvent molecules as a result of hydration of molecular surfaces, particularly around apolar groups, upon dimer dissociation. ΔS_{conf} is the favorable entropic change that arises from the enhancement of conformational degrees of freedom of the backbone and sidechain atoms upon the dissociation of dimer into monomers. The monomers may also undergo some degree of conformational change upon dissociation, which is also likely to contribute favorably to ΔS_{conf}. Finally, ΔS_{mix} is the favorable entropic change due to the enhancement in the translational, rotational and vibrational degrees of freedom of monomers upon dimer dissociation. Several lines of evidence suggest that ΔS_{mix} typically contributes no more than about −10 cal/mol/K of entropy penalty to the overall entropic change upon molecular associations [41–44]. To reverse this statement, one could gain up to +10 cal/mol/K in entropy contributions to the free energy of molecular dissociations. In the case of Grb2 dimer dissociation, the entropic contribution to the free energy is approximately +80 cal/mol/K for the dissociation of each dimer—a value that is much larger than the favorable ΔS_{mix} contribution likely to result from the dissociation of two molecules. On the basis of the foregoing argument, we attribute the favorable entropy gain observed here upon the dissociation of Grb2 dimer into monomers to the increase in the conformational degrees of freedom of backbone and sidechain atoms as embodied in the term ΔS_{conf}.

Enthalpy and entropy have compensatory effects on the temperature-dependency of dimerization

Thermodynamic behavior of monomer–dimer equilibria can be highly dependent on the ambient temperature and knowledge of how thermodynamics vary as a function of temperature can provide invaluable insights into the mechanism of protein oligomerization. In an effort to determine the effect of temperature on the various thermodynamic parameters, we analyzed the dissociation of Grb2 dimer into monomers in the narrow temperature range

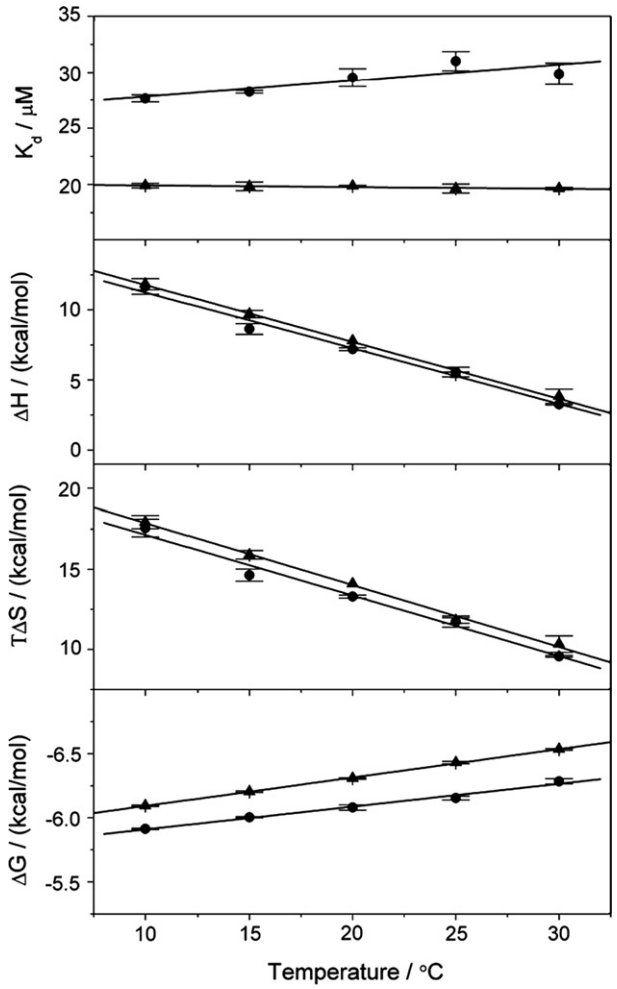

Fig. 3. Dependence of thermodynamic parameters K_d, ΔH, $T\Delta S$ and ΔG on temperature for the dissociation of Grb2 dimer into monomers. Monomer-equivalent Grb2 (100–300 μM) in Tris buffer (●) or Phosphate buffer (▲) in the injection syringe were diluted by making 25× 10 μl injections into the calorimetric cell containing an identical buffer at various temperatures in the range 10–30 °C. To determine the various thermodynamic parameters, the ITC isotherms were fit to the sigmoidal function given by the expression (2). Each data point is the arithmetic mean of 2–3 experiments. All error bars are given to one standard deviation. The solid lines show linear fits to the data points.

10–30 °C (Fig. 3). Our data indicate that both the enthalpic (ΔH) and entropic ($T\Delta S$) contributions to the overall free energy of dissociation (ΔG) show strong temperature-dependence and that both ΔH and $T\Delta S$ largely compensate for each other to generate ΔG that is virtually independent of temperature—while ΔH and $T\Delta S$ experience over 10 kcal/mol change in their contributions to dimer dissociation in going from 10 to 30 °C, ΔG gains no more than 0.5 kcal/mol over the same temperature range. Consistent with this observation is the relatively constant nature of the apparent dissociation constant (~20–30 μM) over the same temperature range. We limited our investigations of the effect of temperature on the thermodynamics of Grb2 dimer dissociation within this narrow temperature range due to a number of technical hurdles; below a temperature of 10 °C, the low signal-to-noise ratio observed is highly undesirable, while above a temperature of 30 °C, the ITC signal in the form of thermal power becomes significantly attenuated such that measurements become less reliable. Despite these limitations, our data suggest that within this temperature range, the dissociation of Grb2 dimer into monomers is overwhelmingly driven by favorable entropic changes accompanied by unfavorable enthalpic contributions to the overall free energy of dissociation.

Table 2
Experimentally determined thermodynamic parameters for the dissociation of Grb2 dimer obtained from ITC measurements at various temperatures in the range 10–30 °C in Tris and Phosphate buffers

	T_H (°C)	T_S (°C)	ΔH_{60} (kcal mol^{-1})	ΔC_p (kcal mol^{-1} K^{-1})
Tris	+38.35 ± 1.10	+55.48 ± 2.50	−8.61 ± 1.13	−0.40 ± 0.03
Phosphate	+39.11 ± 1.79	+58.51 ± 3.36	−8.52 ± 1.45	−0.41 ± 0.03

The values for T_H, the temperature at which ΔH is zero, were obtained from the extrapolation of linear fits to the ΔH versus temperature plots (Fig. 3). The values for T_S, the temperature at which $T\Delta S$ is zero, were obtained from the extrapolation of linear fits to the $T\Delta S$ versus temperature plots (Fig. 3). The values for ΔH_{60}, the enthalpy at 60 °C, were obtained from the extrapolation of linear fits to the ΔH versus temperature plots (Fig. 3). The values for ΔC_p, the heat capacity change, were obtained from the slopes of linear fits to the ΔH versus temperature plots (Fig. 3). Errors were calculated from three to four independent measurements. All errors are given to one standard deviation. Tris buffer was 50 mM Tris, 200 mM NaCl, 1 mM EDTA and 5 mM β-mercaptoethanol at pH 8.0. Phosphate buffer was 50 mM Sodium phosphate, 200 mM NaCl, 1 mM EDTA and 5 mM β-mercaptoethanol at pH 8.0.

The linear and opposing dependence of ΔH and $T\Delta S$ as a function of temperature, while maintaining a more or less constant ΔG, is a common feature observed in protein folding and binding reactions [32,34,45]. This phenomenon gives rise to two key temperature points T_H and T_S—the temperatures where enthalpic (ΔH) and entropic ($T\Delta S$) contributions to the free energy of binding or dissociation change sign, respectively. Thus, in the case of the dissociation of Grb2 dimer into monomers, ΔH will become negative and hence thermodynamically favorable above T_H, while $T\Delta S$ will become negative and hence thermodynamically unfavorable above T_S. Table 2 provides the values for T_H and T_S accompanying the dissociation of Grb2 dimer into monomers. As evidenced in Table 2, T_H for the dissociation of Grb2 into monomers is virtually equal to the physiological temperature of 37 °C within the experimental error of these measurements. This salient observation implies that the dissociation of Grb2 dimer into monomers under physiological temperatures will not be accompanied by unfavorable enthalpic changes and that enthalpic contributions to the free energy of dissociation will become favorable at temperatures above 37 °C. In contrast, the entropic contributions to the free energy of Grb2 dissociation will remain highly favorable at physiological temperatures and may only act in an opposing manner at temperatures greater than about 55 °C.

It is thus interesting to note that while Grb2 dimer dissociation is enthalpically unfavorable at room temperature, the enthalpic contribution to the free energy will become favorable at temperatures above the physiological temperature of 37 °C. At temperatures above 55 °C, enthalpy change will be the sole factor favoring the dissociation of Grb2 dimer into monomers, while at the same time, compensating the unfavorable contributions from entropic changes. The favorable enthalpic contributions to the free energy of dissociation at higher temperatures are likely to result from the increase in the kinetic energy of the system due to lowering of the activation energy for the disruption of intermolecular interactions at the monomer-monomer interface. On the same token, the unfavorable entropic contributions to the free energy of dissociation at higher temperatures most likely arise from the change in the ΔS_{conf} component of the overall entropy change of the system. Unlike at room temperature, the change in ΔS_{conf} is unlikely to be the major factor behind favorable entropic contributions at higher temperatures due to an increase in the kinetic energy of the system; this is likely to cancel out any advantage of monomers over the dimer in terms of the conformational degrees of freedom available to backbone and sidechain atoms at higher temperatures. As a consequence of decreased or negligible contributions from changes in the conformational degrees of freedom available to backbone and sidechain atoms upon dimer dissociation, the hydration of molecular surfaces at the monomer–monomer interface upon dissociation may provide the major source of entropic penalty at higher temperatures.

Grb2 monomers undergo domain swapping upon dimerization

The temperature-dependence of ΔH is related to heat capacity of binding (ΔC_p) by Kirchhoff's relationship $\Delta C_p = d(\Delta H)/dT$; the slope of a plot of ΔH versus temperature equates to ΔC_p. Heat capacity is an important thermodynamic parameter in that it is related to the extent of the burial, occlusion and dehydration of molecular surfaces from surrounding solvent molecules upon intermolecular association. This is technically referred to as the change in solvent-accessible surface area (ΔSASA) [32,46–48]. As such, this information is critical to understanding the mechanism of molecular recognition and, in the context of protein oligomerization, such information can further help us pinpoint any conformational changes involved in the association of protein monomers into dimer.

In an attempt to understand how the association of monomers into dimer affects SASA, we calculated values for ΔC_p in the neighborhood of around −400 cal/mol/K from the slope of ΔH versus temperature plots obtained for the dissociation of Grb2 dimer into monomers (Fig. 3 and Table 2). What might be the significance of such small negative values of ΔC_p observed here? A positive value of ΔC_p implies that the occlusion of polar surfaces dominates the intermolecular association over apolar surfaces [32,49,50]. The fact that ΔC_p possesses small negative values suggests that the occlusion of apolar surfaces does not play a significant role in the dimerization of Grb2. This thermodynamic observation is in stark contrast to the 3D crystal structure of Grb2 dimer, in which protein monomers appear to bury a rather large hydrophobic surface area upon dimerization [29]. Could this discrepancy be due to some sort of protein conformational changes in the monomers upon dimerization? Experimental determination of the magnitude of ΔC_p combined with ΔH_{60} (enthalpy change at 60 °C), as listed in Table 2, has been widely used to quantitatively calculate changes in polar SASA ($\Delta SASA_{polar}$), apolar SASA ($\Delta SASA_{apolar}$) and total SASA ($\Delta SASA_{total}$) upon intermolecular associations [31–34,44,51]. Such changes in SASA upon the dimerization of Grb2 from our thermodynamic measurements are reported in Table 3.

In accordance with the crystal structure of Grb2, whereby the protein crystallized as a dimer with twofold axis of symmetry

Table 3
Changes in polar SASA ($\Delta SASA_{polar}$), apolar SASA ($\Delta SASA_{apolar}$) and total SASA ($\Delta SASA_{total}$) upon the dimerization of Grb2 obtained from thermodynamic and structural data

Method:	Thermodynamic		Structural	
Buffer/model:	Tris	Phosphate	Rigid Body	Flexible Body
$\Delta SASA_{polar}$ (Å^2)	−693	−699	−2070	−964
$\Delta SASA_{apolar}$ (Å^2)	−1553	−1587	−2711	−1432
$\Delta SASA_{total}$ (Å^2)	−2246	−2286	−4781	−2396

ΔSASA values based on thermodynamic data were obtained from the measurement of ΔC_p and ΔH_{60} for the dimer dissociation of Grb2 in Tris and Phosphate buffers (Fig. 3) using expressions (4) and (5), while ΔSASA values based on structural data were derived from 3D structural models of Grb2 dimer and monomer (Fig. 4) using expressions (6) and (7). For ΔSASA values calculated from structural data, two models were assumed—the Rigid Body model and the Flexible Body model. In the Rigid Body model, it was assumed that the monomers undergo no conformational change upon dimerization and that the two monomers essentially come into contact with each other as rigid bodies. In the Flexible Body model, it was assumed that the monomers undergo conformational change and domain swapping upon dimerization (see text for full explanation). ΔSASA values calculated from thermodynamic data make no assumptions and are thus model-independent. Tris buffer was 50 mM Tris, 200 mM NaCl, 1 mM EDTA and 5 mM β-mercaptoethanol at pH 8.0. Phosphate buffer was 50 mM Sodium phosphate, 200 mM NaCl, 1 mM EDTA and 5 mM β-mercaptoethanol at pH 8.0.

[29], the monomers would adopt a rather open conformation particularly with respect to the orientation of the SH2 domain relative to the SH3 domains assuming no conformational change upon dimer dissociation. Given the rather large inter-domain loops (between 13 and 24 residues), the scenario of Grb2 not undergoing any conformational change upon dimer dissociation would be very unrealistic. Rather, a more likely scenario would be the one where the domains undergo some degree of rearrangement relative to each other such that the monomeric protein adopts a more compact and globular shape. To test that this is so, we also determined changes in SASA upon the dimerization of Grb2 from structural data independent of our thermodynamic measurements. To calculate changes in SASA upon the dimerization of Grb2 from structural data, we assumed two models of dimerization—the Rigid Body model and the Flexible Body model. In the Rigid Body model, it was assumed that the monomers do not undergo any conformational change whatsoever upon dimerization and that the domains within each monomer and dimer retain the same conformations relative to each other as those observed in the crystal dimeric unit with twofold axis of symmetry [29]. In the Flexible Body model, it was assumed that the monomers undergo domain swapping upon dimerization so as to preserve the cSH3–SH2 domain–domain interactions.

The Grb2 dimer is largely held together by two major monomer–monomer contacts at the cSH3(A)–SH2(B) and cSH3(B)–SH2(A) interfaces, where A and B in the parenthesis refer to monomers A and B within Grb2 dimer. Given the large and flexible nature of inter-domain loops in Grb2 [52], we reasoned that the cSH3(A)–SH2(B) and cSH3(B)–SH2(A) inter-monomer contacts could be swapped by cSH3(A)–SH2(A) and cSH3(B)–SH2(B) inter-domain contacts within monomers A and B, respectively, upon Grb2 dimer dissociation. In other words, the cSH3–SH2 inter-monomer contacts, between cSH3 domain of one monomer and the SH2 domain of the other monomer and vice versa, that hold the two monomers together to form a dimer could re-establish their respective interactions between cSH3 and SH2 domains within the same monomer due to the flexibility of the inter-domain loops upon Grb2 dimer dissociation. The fact that the cSH3 and SH2 domains are tethered together via a flexible loop (23 residues) implies that the cSH3–SH2 interactions within the same monomer could in fact be much stronger—due to entropic advantage—than the interactions between cSH3 domain of one monomer and SH2 domain of the other monomer and vice versa. Thus, the dimerization of Grb2 would require that the cSH3–SH2 interactions within the same monomer be disrupted and then re-established in an inter-monomer context. The energetic cost of re-building such cSH3–SH2 contacts in an inter-monomer context would then have to be recovered and it may well be that the functional benefits of dimerization outweigh this energetic penalty. Protein dimerization imparts additional advantages, such as enhanced stability and greater specificity, and as such, what may seem Grb2's extravagant pursuit in search of becoming dimerized, could in fact be a blessing in disguise in the context of attaining high fidelity in cellular signaling.

If the Grb2 monomers were to undergo above-mentioned cSH3–SH2 domain swapping, that would involve breaking up of cSH3–SH2 contacts within each monomer and then re-establishing these contacts between the cSH3 domain of one monomer and the SH2 domain of the other monomer, upon dimerization, the extent of the burial of surface area would be expected to be different from the situation where they do not undergo domain swapping and simply come together as rigid bodies. Table 3 summarizes and compares values for $\Delta SASA_{polar}$, $\Delta SASA_{apolar}$ and $\Delta SASA_{total}$ upon the dimerization of Grb2, as calculated from our thermodynamic measurements using ITC and structural data obtained from 3D structural models based on the known crystal structure of Grb2 [29]. Our analysis shows that there are significant deviations between the values calculated from thermodynamic data and the Rigid Body model of dimerization. In contrast, the values determined from thermodynamic data agree par excellence with those calculated from the Flexible Body model. While the changes in SASA determined from thermodynamic data deviate by more than 100% relative to those determined from structural data assuming the Rigid Body model, these values agree within about 10% to those calculated from structural data assuming the Flexible Body model. The small anomalies in the values for changes in SASA between those obtained from thermodynamic data versus those calculated from structural data assuming the Flexible Body model are likely due to errors in the atomic coordinates of the structural models of the monomers; although somewhat similar, the SH2 and SH3 domains may not exactly adopt the orientations relative to each other in the monomers as described by our Flexible Body model. An alternative explanation for the discrepancy observed between the values for changes in SASA between those obtained from thermodynamic data versus those calculated from structural data assuming the Flexible Body model may also be due to poor parameterization of the empirical models that couple heat capacity changes to changes in SASA upon intermolecular associations [31–34,44,51].

In short, we believe that the significant overestimation of changes in SASA calculated from structural data assuming the Rigid Body model are due to the unrealistic assumption that the monomers do not experience any conformational change or domain swapping upon dimerization. This is particularly significant in light of the large flexible inter-domain loops, which are likely to favor cSH3–SH2 domain swapping once the dimer contacts at the monomer–monomer interface are removed. This likely scenario bears fruit in our Flexible Body model, which seems to fully account for our thermodynamic data reported here.

Structural modeling allows rationalization of thermodynamic data

In an attempt to rationalize our thermodynamic data in structural terms, we modeled 3D structures of Grb2 as a dimer and as a monomer that adopts the same conformation as that observed in the dimer structure as well as an alternative conformation consistent with our thermodynamic data discussed above (Fig. 4). All three structures were modeled using the crystal structure of Grb2 dimer as a template [29]. The necessity for modeling the structure of Grb2 dimer arose due to the absence of residues 28–33 in a loop in the nSH3 domain as a result of lack of electron density for these residues in the crystal structure. As evident, in the Grb2 dimer, the two monomers are related by a twofold axis of symmetry and pack tightly against each other burying a total surface area of about 4800 $Å^2$ at the monomer–monomer interface (Fig. 4a). The monomers are largely held together by molecular interaction provided by cSH3 domain of one monomer and SH2 domain of the other monomer at the cSH3(A)–SH2(B) and cSH3(B)–SH2(A) interfaces, where A and B in the parenthesis refer to monomers A and B within Grb2 dimer. Furthermore, the dimer is also stabilized by domain–domain interactions between cSH3 domains from each monomer. However, the nSH3 domains are positioned well away from the monomer–monomer interface and thus do not participate in the dimerization process. Furthermore, such exquisite packing of monomers ensures that the ligand binding pockets of all three domains—nSH3, SH2 and cSH3—in each monomer are solvent-exposed and thus fully accessible to engage in protein–protein interactions with the cellular partners of Grb2.

It has been suggested that the monomers may maintain the same conformation and the relative orientation of their domains when in isolation [29]. However, a quick survey of the monomer conformation suggests that at least some degree of conformational

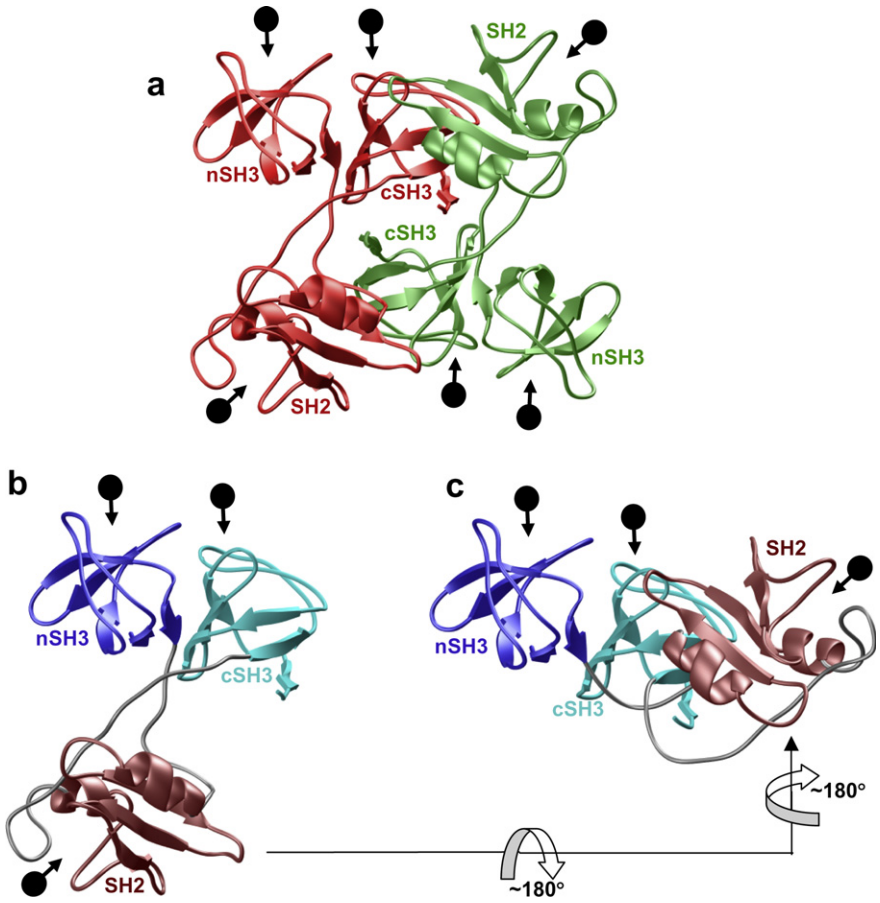

Fig. 4. Three-dimensional modeled structures of Grb2 in dimeric and monomeric forms with arrow-headed black spheres directing the ligand-binding sites within SH2 and SH3 domains. (a) Modeled structure of Grb2 dimer. One monomer is shown in red and the other in green. The three domains nSH3, SH2 and cSH3 are labeled. The structure was modeled using the crystal structure of Grb2 dimer as a template (with a PDB code of 1GRI). The only notable difference in the modeled structure and the crystal structure is the construction of a loop in the nSH3 domain (residues 28–33) that was missing in the crystal structure due to poor electron density. (b) Modeled structure of Grb2 monomer assuming no conformational change upon dimer dissociation. The nSH3 domain is shown in blue, the SH2 domain in brown and the cSH3 domain in cyan. The inter-domain loops nSH3–SH2 and SH2–cSH3 are colored gray. The structure was modeled using only the monomeric unit in the crystal structure of Grb2 dimer as a template (with a PDB code of 1GRI). Additionally, residues 28–33 missing in the crystal structure due to poor electron density were built. (c) Modeled structure of Grb2 monomer assuming conformational change upon dimer dissociation as a result of cSH3–SH2 domain swapping. The nSH3 domain is shown in blue, the SH2 domain in brown and the cSH3 domain in cyan. The inter-domain loops nSH3–SH2 and SH2–cSH3 are colored gray. The structure was modeled using the crystal structure of Grb2 dimer as a template (with a PDB code of 1GRI) but with atomic coordinates derived from only the nSH3 and cSH3 domains of one monomer and the SH2 domain of the other monomer. The residues in the inter-domain loops were allowed to float freely so as enable them to adopt optimal conformations during the modeling process. (For interpretation of the references to color in this figure legend, the reader is referred to the web version of this paper.)

change is likely to occur upon the dissociation of Grb2 dimer. Thus, while the SH3 domains within the monomer are somewhat packed against each other, the SH2 domain makes no contact with either SH3 domain and it is simply held at an interfacial distance of about 30 Å by the nSH3–SH2 loop (13 residues) and the SH2–cSH3 loop (24 residues) (Fig. 4b). If the monomers were to adopt this conformation when in isolation, the flexibility of the inter-domain loops would imply that the SH2 domain is able to adopt multiple orientations and that it could also yo–yo relative to the SH3 domains. This hypothesis is further supported by our heat capacity measurements, which suggest that the total surface area buried upon Grb2 dimerization is close to 2300 Å^2 instead of 4800 Å^2 obtained from structural analysis alone assuming no conformational changes in the monomers upon Grb2 dimerization (Table 3). In light of the foregoing argument, the most straightforward interpretation of this discrepancy is that the SH2 domain is unlikely to be fully solvent-exposed and most likely packs against either the nSH3 domain or the cSH3 domain or both in the isolated monomers. Given that the cSH3-SH2 domain-domain interactions appear to be the dominant force holding the monomers together into a dimer, it is plausible to speculate that the cSH3 and SH2 domains could also re-establish such contact in the context of an isolated monomer (Fig. 4c). To paraphrase this slightly, the SH2 domain may pack against the cSH3 domain within the same isolated monomer in a manner akin to the domain-domain interactions observed between the SH2 domain of one monomer and the cSH3 domain of the other monomer within the Grb2 dimer. To accomplish such domain swapping, the SH2 domain will have to undergo two spatial transformations; to rotate clockwise by ~180° about an axis parallel to the nSH3–cSH3 plane followed by a second clockwise rotation of ~180° about an axis perpendicular to the nSH3–cSH3 plane (Fig. 4b and c). The large and flexible nature of inter-domain loops nSH3–SH2 and SH2–cSH3 would ensure that this is not only kinetically feasible but the tethering of SH2 and cSH3 domains within the same isolated monomer would also be entropically more favorable than the coming together of SH2 domain of one monomer and the cSH3 domain of the other monomer in the context of a dimer.

In so doing, the SH2–cSH3 packing within each isolated monomer would bury surface area of approximately 1200 Å^2 at the domain–domain interface, or a total surface area of about 2400 Å^2 between two isolated monomers. Thus, upon Grb2 dimerization, the disruption of SH2–cSH3 contacts within both isolated monomers would initially result in the exposure of surface area of about

2400 Å^2 and hence a deficit of surface area of about 2400 Å^2 prior to re-establishing the SH2–cSH3 contacts across each monomer to generate the dimer in order to pay for this deficit. The total surface area buried upon Grb2 dimerization is about 4800 Å^2 assuming no conformational change in the monomers. However, after paying a deficit of surface area of about 2400 Å^2 exposed upon the disruption of SH2–cSH3 contacts within each isolated monomer, the overall surface area buried upon Grb2 dimerization would equate to about 4800 Å^2 minus 2400 Å^2. Thus, a value of 2400 Å^2 would be expected to be the overall burial of surface area being recorded in our heat capacity measurements reported here. A value of about 2300 Å^2 deduced from such measurements is in an excellent agreement with a value of 2400 Å^2 derived from structural data for Grb2 dimerization on the basis of the assumption that such dimerization proceeds via cSH3–SH2 domain swapping. Such conformational change that Grb2 may have to undergo upon dimerization, in agreement with our thermodynamic data reported here, can be best visualized in the form of a movie accessible at http://labs.med.miami.edu/farooq/movies/Grb2Dimer.

It should be noted here that the isolated SH2 domain of Grb2 can also dimerize by virtue of its ability to undergo domain swapping [53–55]. Here, the dimerization is achieved through the ability of the C-terminal α-helix from each SH2 domain to swap in an inter-domain manner so as to generate an intertwined SH2 dimer that exhibits lower affinity for cognate ligands relative to SH2 monomer. This observation is in contrast to the model presented above for the dimerization of Grb2 in which the SH2 domain simply swaps its interactions with the cSH3 domain from being in an intra-molecular contact in the context of Grb2 monomer to being in an inter-molecular contact in the Grb2 dimer without blocking access to ligand binding sites. Although ligand binding affinity to SH2 and SH3 domains has not been measured in the context of full-length protein, it is unlikely that Grb2 dimerization would lower the ligand binding affinity in a manner akin to that observed for the SH2 domain-swapped dimer. On the contrary, the SH2 and SH3 domains in the context of Grb2 dimer are likely to bind with much higher affinity to multivalent ligands due to entropic advantage. That such a scenario may prevail warrants further studies on the role of Grb2 dimerization in cellular signaling.

Conclusions

Elucidating protein–protein interactions in thermodynamic terms offers molecular insights into the mechanisms of life at a level second to none. Although Grb2 has been perceived as a central player in cellular signaling since its discovery over a decade ago [2,4,29], little is known about the role of oligomerization in the biological function of Grb2. This is particularly significant given that Grb2 is one of only a handful of adaptor modular proteins for which complete 3D structure has been solved to atomic resolution and it is often tipped as the best characterized adaptor protein in cellular signaling [29]. The ability of proteins to undergo oligomerization comes at a price but that is worth paying for in exchange for functional advantages that include but are not limited to enhanced stability, greater specificity and selectivity toward cognate ligands, and increased ability to participate in signal amplification—a feature that is a hallmark of cellular signaling and perturbations to which can make the difference between a healthy and diseased cell.

In this study, using an array of biophysical methods, we have shown that Grb2 exists in a dynamic equilibrium between dimer and monomers with the equilibrium well in favor of the latter species under low protein concentrations that are likely to be encountered under normal functioning of the cellular machinery. Although the Grb2 monomer–dimer equilibrium is likely to be in favor of the monomer in quiescent cells, rapid expression and rise in Grb2 concentration upon mitogenic stimulation is likely to shift this equilibrium in favor of the dimer. Other factors within the cell are also likely to affect the Grb2 monomer–dimer equilibrium. Studies on cultured mammalian cells indicate that phosphorylation of both Y239 and Y317 in p52Shc is required for efficient formation of p52Shc–Grb2–Sos complex [10]. Thus, the requirement of two rather than one phosphorylation site in p52Shc for Grb2 recruitment may shift the Grb2 monomer–dimer equilibrium in favor of the dimer due to the fact that SH2 domains in dimeric Grb2 are likely to bind to two phosphorylation sites in p52Shc with much greater affinity and specificity than a single SH2 domain in monomeric Grb2 and as a consequence of this differential binding, the existence of Grb2 dimer over monomers will be highly favored over both thermodynamic and kinetic grounds not to mention the functional advantages that such a mechanism may impart upon cellular signaling.

Our study also demonstrates exquisitely how thermodynamic information can be employed to corroborate or refute structural data. Although Grb2 crystallizes as a dimer with a twofold axis of symmetry [29], the assumption that the monomers within this dimer may retain the same conformation in isolation is unlikely to bear fruit due to the large and flexible inter-domain loops. Our thermodynamic data indeed suggest strongly that the monomers are likely to undergo cSH3–SH2 domain swapping and thus adopt a more compact structure than that observed in the Grb2 dimer. Given that the structure of Grb2 in its monomeric state is not available and that it may not be practically surmountable in the foreseeable future due to the requirement of protein at high concentrations, conditions under which it predominantly exists as a dimer, for structural analysis by both the X-ray and NMR methodologies, the relevance of our thermodynamic studies presented here could not be overemphasized.

In short, our data demonstrate unequivocally that Grb2 exists in monomer-dimer equilibrium in solution and that it is likely to undergo cSH3–SH2 domain swapping upon dimerization. This salient observation has profound impacts for furthering our understanding of the role of Grb2 in cellular signaling and for the possible therapeutic intervention of Grb2 in signaling cascades that result in oncogenic transformation of cells. Many drugs are designed to interfere with protein oligomerization or lead to disruption of protein–protein interfaces. Our demonstration that Grb2 exists in monomer–dimer equilibrium may open up new avenues of drug design for disrupting Grb2 dimerization, such as targeting the monomeric conformation of Grb2 so as to prevent its dimerization, and thus could lead to the development of novel anti-cancer drugs with low toxicity coupled with more effectiveness.

Acknowledgments

This work was supported by funds from the UM/Sylvester Braman Family Breast Cancer Institute and the American Heart Association Grant (#0655087B) to A.F.

References

[1] A.M. Cheng, T.M. Saxton, R. Sakai, S. Kulkarni, G. Mbamalu, W. Vogel, C.G. Tortorice, R.D. Cardiff, J.C. Cross, W.J. Muller, T. Pawson, Cell 95 (1998) 793–803.
[2] P. Chardin, D. Cussac, S. Maignan, A. Ducruix, FEBS Lett. 369 (1995) 47–51.
[3] M. Rozakis-Adcock, J. McGlade, G. Mbamalu, G. Pelicci, R. Daly, W. Li, A. Batzer, S. Thoma, J. Brugge, P.G. Pelicci, J. Schlessinger, T. Pawson, Nature 360 (1992) 689–692.
[4] E.J. Lowenstein, R.J. Daly, A.G. Batzer, W. Li, B. Margolis, R. Lammers, A. Ullrich, E.Y. Skolnik, D. Bar-Sagi, J. Schlessinger, Cell 70 (1992) 431–442.
[5] M. Rozakis-Adcock, J. McGlade, G. Mbamalu, G. Pelicci, R. Daly, W. Li, A. Batzer, S. Thomas, J. Brugge, P.G. Pelicci, et al., Nature 360 (1992) 689–692.
[6] M. Rozakis-Adcock, R. Fernley, J. Wade, T. Pawson, D. Bowtell, Nature 363 (1993) 83–85.

[7] S.F. Walk, M.E. March, K.S. Ravichandran, Eur. J. Immunol. 28 (1998) 2265–2275.
[8] R.A. Blake, M.A. Broome, X. Liu, J. Wu, M. Gishizky, L. Sun, S.A. Courtneidge, Mol. Cell. Biol. 20 (2000) 9018–9027.
[9] J. McGlade, A. Cheng, G. Pelicci, P.G. Pelicci, T. Pawson, Proc. Natl. Acad. Sci. USA 89 (1992) 8869–8873.
[10] S.L. Harmer, A.L. DeFranco, Mol. Cell. Biol. 17 (1997) 4087–4095.
[11] P. Chardin, J.H. Camonis, N.W. Gale, L. van Aelst, J. Schlessinger, M.H. Wigler, D. Bar-Sagi, Science 260 (1993) 1338–1343.
[12] N. Li, A. Batzer, R. Daly, V. Yajnik, E. Skolnik, P. Chardin, D. Bar-Sagi, B. Margolis, J. Schlessinger, Nature 363 (1993) 85–88.
[13] U. Schaeper, N.H. Gehring, K.P. Fuchs, M. Sachs, B. Kempkes, W. Birchmeier, J. Cell Biol. 149 (2000) 1419–1432.
[14] M. Lewitzky, C. Kardinal, N.H. Gehring, E.K. Schmidt, B. Konkol, M. Eulitz, W. Birchmeier, U. Schaeper, S.M. Feller, Oncogene 20 (2001) 1052–1062.
[15] K. Seedorf, G. Kostka, R. Lammers, P. Bashkin, R. Daly, W.H. Burgess, A.M. van der Bliek, J. Schlessinger, A. Ullrich, J. Biol. Chem. 269 (1994) 16009–16014.
[16] M. Vidal, J.L. Montiel, D. Cussac, F. Cornille, M. Duchesne, F. Parker, B. Tocque, B.P. Roques, C. Garbay, J. Biol. Chem. 273 (1998) 5343–5348.
[17] H. Odai, K. Sasaki, A. Iwamatsu, Y. Hanazono, T. Tanaka, K. Mitani, Y. Yazaki, H. Hirai, J. Biol. Chem. 270 (1995) 10800–10805.
[18] R.K. Park, W.T. Kyono, Y. Liu, D.L. Durden, J. Immunol. 160 (1998) 5018–5027.
[19] S.J. Moeller, E.D. Head, R.J. Sheaff, Mol. Cell. Biol. 23 (2003) 3735–3752.
[20] G.W. Reuther, C.J. Der, Curr. Opin. Cell Biol. 12 (2000) 157–165.
[21] M.J. Robinson, M.H. Cobb, Curr. Opin. Cell Biol. 9 (1997) 180–186.
[22] J.M. Cunnick, S. Meng, Y. Ren, C. Desponts, H.G. Wang, J.Y. Djeu, J. Wu, J. Biol. Chem. 277 (2002) 9498–9504.
[23] H. Gu, B.G. Neel, Trends Cell Biol. 13 (2003) 122–130.
[24] T. Araki, H. Nawa, B.G. Neel, J. Biol. Chem. 278 (2003) 41677–41684.
[25] D. Kim, J. Chung, J. Biochem. Mol. Biol. 35 (2002) 106–115.
[26] R.B. Vallee, J.S. Herskovits, J.G. Aghajanian, C.C. Burgess, H.S. Shpetner, Ciba Found. Symp. 176 (1993) 185–193. discussion 193–187.
[27] J.S. Herskovits, C.C. Burgess, R.A. Obar, R.B. Vallee, J. Cell Biol. 122 (1993) 565–578.
[28] T. Ravid, J.M. Heidinger, P. Gee, E.M. Khan, T. Goldkorn, J. Biol. Chem. 279 (2004) 37153–37162.
[29] S. Maignan, J.P. Guilloteau, N. Fromage, B. Arnoux, J. Becquart, A. Ducruix, Science 268 (1995) 291–293.
[30] E. Gasteiger, C. Hoogland, A. Gattiker, S. Duvaud, M.R. Wilkins, R.D. Appel, A. Bairoch, Protein identification and analysis tools on the ExPASy server, in: J.M. Walker (Ed.), The Proteomics Protocols Handbook, Humana Press, Totowa, New Jersey, USA, 2005, pp. 571–607.
[31] S.P. Edgcomb, K.P. Murphy, Curr. Opin. Biotechnol. 11 (2000) 62–66.
[32] K.P. Murphy, E. Freire, Adv. Protein Chem. 43 (1992) 313–361.
[33] D. Xie, E. Freire, Proteins 19 (1994) 291–301.
[34] R.S. Spolar, J.M.T. Record, Science 263 (1994) 777–784.
[35] R. Fraczkiewicz, W. Braun, J. Comput. Chem. 19 (1998) 319–333.
[36] M.A. Marti-Renom, A.C. Stuart, A. Fiser, R. Sanchez, F. Melo, A. Sali, Annu. Rev. Biophys. Biomol. Struct. 29 (2000) 291–325.
[37] M. Carson, J. Appl. Crystallogr. 24 (1991) 958–961.
[38] D. McPhail, A. Cooper, J. Chem. Soc. Faraday Trans. 93 (1997) 2283–2289.
[39] S.D. Burrows, M.L. Doyle, K.P. Murphy, S.G. Franklin, J.R. White, I. Brooks, D.E. McNulty, M.O. Scott, J.R. Knutson, D. Porter, et al., Biochemistry 33 (1994) 12741–12745.
[40] A. Cooper, Microcalorimetry of Protein-Protein Interactions, in: J.E. Ladbury, B.Z. Chowdhry (Eds.), Biocalorimetry: Applications of Calorimetry in the Biological Sciences, John Wiley & Sons Ltd, New York, 1998, pp. 103–111.
[41] X. Siebert, L.M. Amzel, Proteins 54 (2004) 104–115.
[42] K.P. Murphy, D. Xie, K.S. Thompson, L.M. Amzel, E. Freire, Proteins 18 (1994) 63–67.
[43] A. Tamura, P.L. Privalov, J. Mol. Biol. 273 (1997) 1048–1060.
[44] K.P. Murphy, Med. Res. Rev. 19 (1999) 333–339.
[45] K.P. Murphy, V. Bhakuni, D. Xie, E. Freire, J. Mol. Biol. 227 (1992) 293–306.
[46] P.L. Privalov, S.J. Gill, Adv. Protein Chem. 39 (1988) 191–234.
[47] R.S. Spolar, J.H. Ha, M.T. Record Jr., Proc. Natl. Acad. Sci. USA 86 (1989) 8382–8385.
[48] J.E. Ladbury, J.G. Wright, J.M. Sturtevant, P.B. Sigler, J. Mol. Biol. 238 (1994) 669–681.
[49] P.L. Privalov, G.I. Makhatadze, J. Mol. Biol. 224 (1992) 715–723.
[50] R.S. Spolar, J.R. Livingstone, M.T. Record Jr., Biochemistry 31 (1992) 3947–3955.
[51] E. Freire, Arch. Biochem. Biophys. 303 (1993) 181–184.
[52] S. Yuzawa, M. Yokochi, H. Hatanaka, K. Ogura, M. Kataoka, K. Miura, V. Mandiyan, J. Schlessinger, F. Inagaki, J. Mol. Biol. 306 (2001) 527–537.
[53] N. Schiering, E. Casale, P. Caccia, P. Giordano, C. Battistini, Biochemistry 39 (2000) 13376–13382.
[54] P. Nioche, W.Q. Liu, I. Broutin, F. Charbonnier, M.T. Latreille, M. Vidal, B. Roques, C. Garbay, A. Ducruix, J. Mol. Biol. 315 (2002) 1167–1177.
[55] A.P. Benfield, B.B. Whiddon, J.H. Clements, S.F. Martin, Arch. Biochem. Biophys. 462 (2007) 47–53.